Lattice Boltzmann simulation of the two-dimensional Rayleigh-Taylor instability

Xiaobo Nie,[1,2,3] Yue-Hong Qian,[1] Gary D. Doolen,[2] and Shiyi Chen[2]
[1]*Department of Applied Physics and Applied Mathematics, Columbia University, New York, New York 10027*
[2]*Theoretical Division and Center for Nonlinear Studies, National Laboratory, Los Alamos, New Mexico 87545*
[3]*Institute of Applied Physics and Computational Mathematics, Beijing 100088, China*
(Received 19 May 1998)

A lattice Boltzmann model for multicomponent fluid flows is used to simulate the two-dimensional Rayleigh-Taylor instability. The dynamical processes of the instability, varying from linear growth to mixing, have been simulated. The results agree with experiments, analytical studies, and other numerical simulations. [S1063-651X(98)03811-2]

PACS number(s): 47.20.Ma, 05.50.+q, 02.70.−c

The Rayleigh-Taylor (RT) instability occurs when a low-density fluid pushes a high-density fluid or a heavy fluid lies above a light fluid in a gravitational field [1]. This problem continues to attract attention partly because of its role in understanding inertial confinement fusion [2,3]. Analytic methods, including perturbation methods, are mostly valid in the linear region and turbulent models are mostly applied in the mixing region. Direct numerical simulation (DNS), which solves the dynamic fluid equations, is able to study processes related to the Rayleigh-Taylor instability, but its usefulness is limited by computational power. Recently, DNS of the Rayleigh-Taylor instability became feasible because of the emergence of high-performance computers. Youngs [4–6], Glimm *et al.* [7], and Li [8,9] simulated the RT instability using marker-and-cell, front-tracking, and level-set methods. The simulations reveal much useful information which has helped in the understanding of the growth of the instability.

The lattice gas [10] and the lattice Boltzmann methods [11] are novel numerical schemes based on mesoscopic dynamics which provide alternatives to traditional numerical techniques for simulating fluid flows [12]. These methods can simulate the macroscopic equations accurately and efficiently, and also preserve some of the advantages of kinetic equations, including easy programming in parallel computers and accurately simulating flows with complicated wall geometries and interfaces. Gunstensen *et al.* [13] simulated the Rayleigh-Taylor instability using a two-phase lattice-gas model. Lattice Boltzmann methods for multiphases and multicomponents have been developed by Gunstensen *et al.* [14], Shan and Chen [15], and Swift *et al.* [16].

In this paper we extend the multicomponent model of Gunstensen *et al.* [14] and Grunau *et al.* [17] for studying the two-dimensional Rayleigh-Taylor instability. A square lattice with multiple speeds is used. Let us define $f_i(\mathbf{x},t)$ as the total particle density distribution, at $\mathbf{x}$ and time t with velocity $\mathbf{c_i}$. Here $f_i=f_i^1+f_i^2$, $i=1,\ldots,9$ for the D2Q9 model [18] or $i=1,\ldots,13$ for the D2Q13 [19] model. The velocity $\mathbf{c_i}$ includes eight vectors along the links of the square lattice and a zero velocity for the D2Q9 model. D2Q13 also includes four velocities with speed 2 (in lattice units). These velocities are (0,0), ($\pm$1,0), (0,$\pm$1), ($\pm$1, $\pm$1), ($\pm$2,0), and (0,$\pm$2). The lattice Boltzmann equation for fluids can be written as

$$f_i^l(\mathbf{x}+\mathbf{c_i},t+1)-f_i^l(\mathbf{x},t)=(\Omega_i^l)^1+(\Omega_i^l)^2-\frac{t_p\mathbf{G}\cdot\mathbf{c_i}}{c_d}, \quad (1)$$

where t_p and c_d are constants, the index l refers to either the first or the second fluid, and the index p equals c_i^2. For the first part of the collision operator we use the Bhatnager-Gross-Krook (BGK) approximation [20–22,18,23]

$$(\Omega_i^l)^1=-\frac{1}{\tau}(f_i^l-f_i^{l(\mathrm{eq})}), \quad (2)$$

which represents the process of relaxation to local equilibrium, where $f_i^{l(\mathrm{eq})}$ is the local equilibrium distribution function and τ is the relaxation time. One suitable equilibrium distribution function leading to the Navier-Stokes equations is [18]

$$f_i^{l(\mathrm{eq})}=r_p^l\rho+t_p\rho\left[\frac{c_{i\alpha}u_\alpha}{c_d^2}+\frac{(c_{i\alpha}c_{i\beta}-c_d^2\delta_{\alpha\beta})}{2c_d^4}u_\alpha u_\beta\right]. \quad (3)$$

Here c_d^2, t_p, and r_p^l are listed in Table I, where c_l ($l=1,2$) are acoustic speeds of the two fluids. The greek subscripts α and β denote the spatial directions in Cartesian coordinates. The total density ρ, the densities of two fluids, ρ_1 and ρ_2, and the macroscopic velocity, $\mathbf{u}$, are defined by $\rho=\rho_1+\rho_2$, $\rho_1=\Sigma_i f_i^1$, $\rho_2=\Sigma_i f_i^2$, $\rho\mathbf{u}=\Sigma_i\mathbf{c_i}f_i$.

The second part of the collision operator [14,17] in Eq. (1) is defined as follows:

$$(\Omega_i^l)^2=\frac{a}{4}\frac{t_p}{t_1}|\mathbf{F}|\left(\frac{2(\mathbf{c_i}\cdot\mathbf{F})^2}{c_i^2F^2}-1\right), \quad (4)$$

where $\mathbf{F}(\mathbf{x})=\Sigma_i\mathbf{c_i}[\rho_1(\mathbf{x}+\mathbf{c_i})-\rho_2(\mathbf{x}+\mathbf{c_i})]$ is the local color gradient, and a is a free parameter which is linearly proportional to the surface tension. $\mathbf{G}$ is a vector representing an external force. To maintain the interface between fluids, we follow Gunstensen's scheme [14] to redistribute the particles

TABLE I. The parameters in the equilibrium distribution function.

Model	c_d^2	t_0	t_1	t_2	t_4	r_0^l	r_1^l	r_2^l	r_4^l
D2Q9	$\frac{1}{3}$	$\frac{4}{9}$	$\frac{1}{9}$	$\frac{1}{36}$		$1-\frac{5}{3}c_l^2$	$\frac{1}{3}c_l^2$	$\frac{1}{12}c_l^2$	
D2Q13	$\frac{2}{5}$	$\frac{2}{5}$	$\frac{7}{5}$	$\frac{1}{25}$	$\frac{1}{300}$	$1-\frac{3}{2}c_l^2$	$\frac{4}{15}c_l^2$	$\frac{1}{10}c_l^2$	$\frac{1}{120}c_l^2$

after each collision step in a way that maximizes the quantity $(\Sigma_i \mathbf{c_i} f_i^1)\cdot\mathbf{F}$, while requiring that ρ_1, ρ_2, and $f_i(\mathbf{x},t)$ are conserved at each site.

Using the Chapman-Enskog multiscale technique [12], we can obtain the following macroscopic dynamical equations in the low Mach number or the nearly incompressible limit:

$$\partial_t \rho + \partial_\alpha(\rho u_\alpha) = 0, \tag{5}$$

$$\partial_t(\rho u_\alpha) + \partial_\beta(\rho u_\alpha u_\beta) = -\partial_\alpha p - \partial_\beta \pi_{\alpha\beta} - G_\alpha, \tag{6}$$

$$p = c_1^2\rho_1 + c_2^2\rho_2 + p', \quad \pi_{\alpha\beta} = \nu\rho(\partial_\alpha u_\beta + \partial_\beta u_\alpha).$$

Here viscosity $\nu = c_d^2/2(2\tau - 1)$ and $p' \sim |\nabla\cdot\mathbf{F}|$ are zero except in the interface between the two fluids, creating the effects of surface tension. Using the definition of mechanical surface tension, and after some algebra, we obtain an analytic formula for the surface tension: $\sigma = 12a\tau\rho$ or $42a\tau\rho$ for the D2Q9 or the D2Q13 model, respectively. We point out that we have multiplied by the proper factor t_p in Eq. (4) for each velocity in order to obtain an isotropic surface tension. For example, for the D2Q13 model, $\sigma = 42a\tau\rho g(\theta_f)$, where $g(\theta_f) = \frac{1}{6}\Sigma_i i c_i^4 (t_p/t_1)\cos^2(2\theta_i - 2\theta_f) = 1$. Here θ_f is the angle between the x axis and the normal of the interface and θ_i is the angle between the x axis and $\mathbf{c_i}$. It is the proper choice factors that make $g(\theta_f)$ constant. This is an important extension of the single-speed multiphase model.

Numerical simulations of the Rayleigh-Taylor instability have been carried out using the above two lattice Boltzmann models. First, the linear growth rate was checked for the D2Q9 model. In the simulation we set $\mathbf{G} = -\rho g \mathbf{e_y}$ to provide the gravitational acceleration, g, along the negative y axis. Initially, a fluid of density ρ_1 rests on the top of another fluid of density $\rho_2 (\rho_1 > \rho_2)$. To get the correct pressure for the stationary fluid, we take $c_2 = c_d$, $c_2 = (\rho_2/\rho_1)c_d$. A small perturbation $y(x) = y_0 \cos(kx)$ is added at the interface, where $y_0 \leqslant 0.02\lambda$, the wave number $k = 2\pi/\lambda$, and λ is the wavelength of the perturbation. The height of the fluid in the vertical or y direction, H, satisfies $Hk \gg 1$. Periodic boundary conditions are used in the horizontal direction and smooth wall conditions are used at the top and bottom. The linearly perturbed solution of Eqs. (4) and (5) in the incompressible limit predicts that the amplitude of perturbation increases with time [3],

$$h(t) = a_0 e^{\gamma t} + b_0 e^{-\gamma' t},$$

where a_0, b_0 satisfy $a_0 + b_0 = y_0$, $a_0\gamma - b_0\gamma' = 0$, and $\gamma, \gamma' \geqslant 0$. γ is the linear growth rate and satisfies the dispersion relation,

$$4\gamma k + [-\alpha + (\rho_1+\rho_2)\gamma^2]\left(\frac{1}{\mu_1 k + \sqrt{\mu_2^2 k^2 + \mu_2\rho_2\gamma}} + \frac{1}{\mu_2 k + \sqrt{\mu_1^2 k^2 + \mu_1\rho_1\gamma}}\right) = 0, \tag{7}$$

where $\mu_l = \rho_l \nu_l$, $\alpha = (\rho_1 - \rho_2)kg - k^3\sigma$.

Figure 1 shows a comparison of the linear theory with numerical results. In the simulation, we have taken $g = 0.25 \times 10^{-4}$, $\tau = 1$, $\rho_1 = 3$, and $\rho_2 = 1$. The agreement between theory and the lattice Boltzmann simulation is reasonably good. However, a small difference is observed and the difference seems to increase with increasing of the wave number. We do not have insight at this stage about this difference.

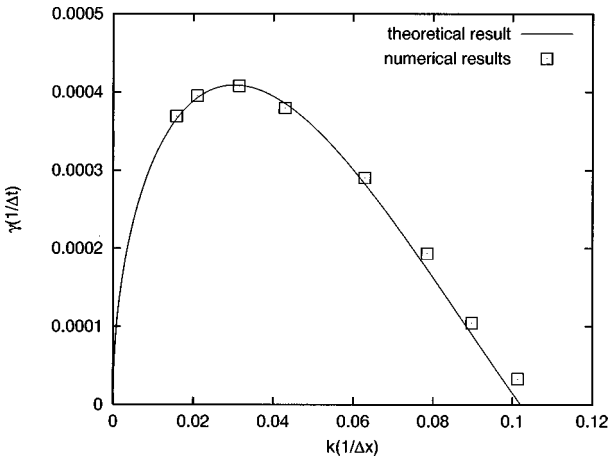

FIG. 1. The growth rate γ vs the wave number k. Δx is the lattice spacing and Δt is the time increment.

The dynamics of this flow can be described by five dimensionless parameters: the Atwood number, $A = (\rho_1 - \rho_2)/(\rho_1 + \rho_2)$; the Reynolds number, $R_e = LV/\nu$; the Euler number, $E = P/(\rho V^2)$; the Froude number, $F_e = V^2/(gL)$; and the Strouhal number, $S_t = L/(TV)$. L, T, V, P, and ρ are the characteristic length, time, speed, pressure, and density. Figure 2 shows the evolution of interfaces using the D2Q13 model with $g = 10^{-4}$, $\nu = 0.2$, $\rho_1 = 3$, $\rho_2 = 1$, $\sigma = 0$, $\lambda = 60$ and the D2Q9 model with the same five dimensionless parameters for times at $\gamma t = 5$, 10, and 18, for which the linear growth rate is $\gamma = 0.917 \times 10^{-3}$. As shown in Figs. 2(a) and 2(b), the sinusoidal perturbation grows initially and then changes into a round-topped bubble, and then the light fluid rises into the heavy fluid and spikes formed by the heavy fluid fall into the light fluid. As the spike falls, the Helmholtz instability along the edges of the spike induces a mushroom-

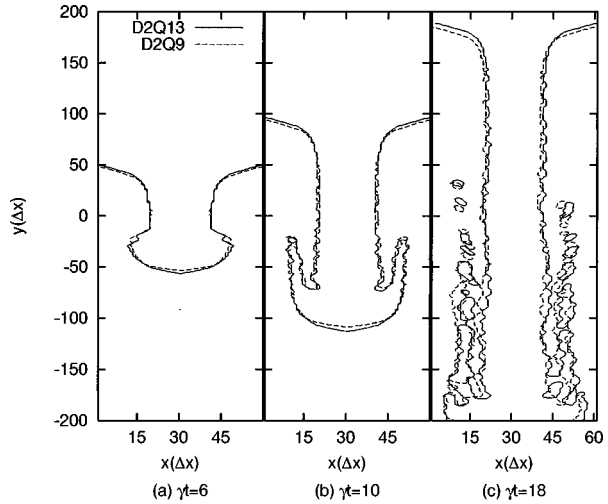

FIG. 2. Interface evolution for the RT instability at $\gamma t = 6$, 10, and 18. The solid curve is the result for the D2Q13 model and the dashed curve for the D2Q9 model.

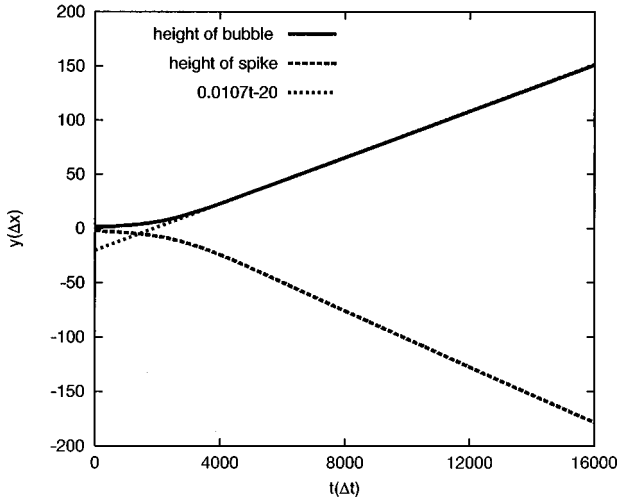

FIG. 3. Heights of the bubble and the spike as a function of time.

like flow pattern. This result agrees with the results of a finite difference code using the front tracking method [4,5,7]. Finally, in Fig. 2(c) the mushroom breaks and drops are formed. At this stage of the instability the interface is very complicated. It is difficult to track these complex motions using conventional numerical methods. It can also be seen that the results of the two models agree well. This further confirms the reliability of the lattice BGK model (1)–(4).

Figure 3 shows the time evolution of the height of the heavy fluid moving into the light fluid and the height of the light fluid moving into the heavy fluid using D2Q13. Initially the heights grow exponentially. Then, after a transition, the bubble rises with constant velocity. This agrees qualitatively with Taylor's experiments. Taylor derived an empirical formula for the bubble velocity: $V_b = C\sqrt{Agr}$, where $C = 0.32$ and r is the bubble radius. Taking $r = \lambda/2$, the Taylor formula gives $V_b = 0.0124$, which is to be compared with the best fit in Fig. 3, $V_b = 0.0107$. It should be pointed out that in the Taylor experiment, the dimensionless parameter $R = \nu k^2/\gamma$ is much smaller than 1, whereas in our numerical simulation R equals 2 due to the relatively large viscosity in the lattice Boltzmann model. The difference in the growth velocity could be attributed to the different values of R used.

Finally, we simulated the growth of the instability from random initial perturbations. The perturbation is $h = \Sigma_n a_n \cos(k_n x) + b_n \sin(k_n x)$, $k_n = 2\pi n L_x^{-1}$. Here L_x is the length of the simulation domain in the x or horizontal direction and a_n, b_n were chosen at random from a Gaussian distribution, $n \subset [n_{\min}, n_{\max}]$. We have chosen the two fluids to have the same density (for better numerical stability) in this simulation, but they are subjected to different body forces, $\rho_1 = \rho_2$ and $\mathbf{G} = -(g_1\rho_1 + g_2\rho_2)\mathbf{e_y}$. This can be considered to be the ideal limit of the Rayleigh-Taylor instability when ρ_1 approaches ρ_2 but g approaches infinity in such a way that the difference in the gravitational force remains constant. We set $g_1 = -g_2 = g$, although this is not required.

Two simulations were run with 300×300 points, $g = 0.5 \times 10^{-4}$, $n_{\min} = 1$, $n_{\max} = 30$, and $\nu = 1/30$ or $1/1500$. Figure 4 shows the location of the interfaces at $gt^2 = 50$, 450, and 1250 for $\nu = 1/1500$. Because of interactions between bubbles and drops, the dominant wavelength of the interface

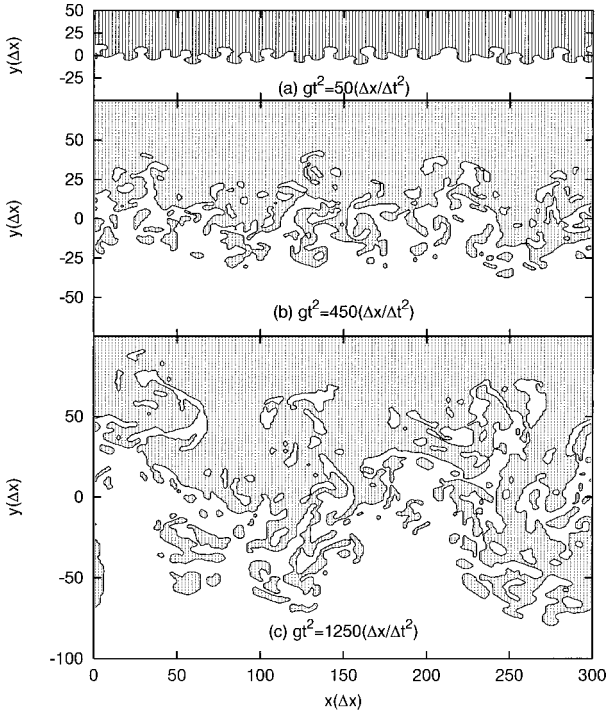

FIG. 4. Interface at (a) $gt^2 = 50$, (b) $gt^2 = 450$, and (c) $gt^2 = 1250$ for $\nu = 1/1500$.

increases from $\approx L_x/25$ to $\approx L_x/2$ at the end of the simulation. This phenomenon agrees with the results of Youngs [4,5] using MAC methods or Van Leer methods. In our results, there are more small droplets near the interface. This difference may come from the fact that we use the same density for both fluids.

Figure 5 shows the width of the mixing region as a function of gt^2 for two viscosities. The mixing region is defined as the region in which the average concentration of one of the fluids is in the range 0.01 to 0.99. The widths are approximately linear functions of gt^2. This result is similar to earlier experimental and theoretical results [24,4,5,7,25,8].

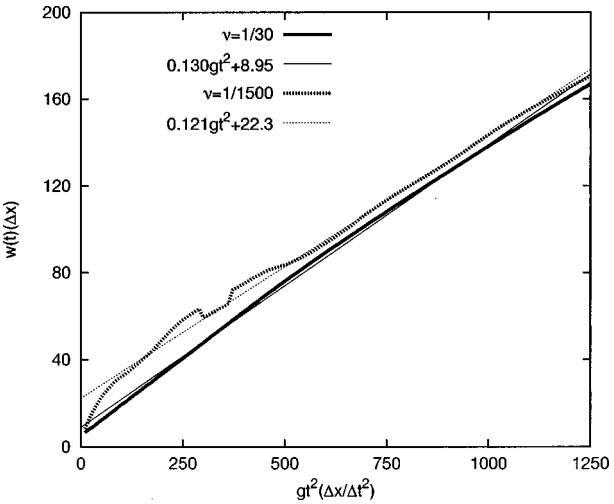

FIG. 5. Width of the mixing region as a function of gt^2. The straight lines were obtained by fitting the formulas described in the text.

The depth to which the light fluid enters the heavy fluid is given by

$$h(t)=\alpha A g t^2+h_0, \tag{8}$$

where h_0 and α are constants. α is found to be insensitive to the density ratio. The experiments gave an α of 0.6 to 0.7 and theoretical studies including numerical simulations gave an α of 0.4 to 0.7. It is difficult to compare our numerical results with the above equations quantitatively because our simulations assumed $\rho_1=\rho_2$. A reasonable generalization of Eq. (8) is

$$h(t)=\alpha\frac{\rho_1 g_1-\rho_2 g_2}{\rho_1+\rho_2}t^2+h_0.$$

When $g_1=g_2=g$, Eq. (8) is recovered. Assuming $g_1=-g_2=g$, $\rho_1=\rho_2$, and $w=2h$, the above equation becomes

$$w(t)=2\alpha g t^2+2h_0.$$

We fit the numerical results of the mixing width using this equation. These fits are included in Fig. 5. The values of α are 0.65 and 0.61, respectively. These numbers agree well with experiments and other theoretical results. Of course this is not a direct comparison.

In this paper, we have applied a lattice Boltzmann model based on a previous multicomponent model to simulate the Rayleigh-Taylor instability. The linear growth rate agrees with analytic solutions for incompressible fluids. The single bubble dynamics agrees with experiments and other methods qualitatively. The velocity of the bubble is close to that of an incompressible ideal fluid. The instability caused by random initial perturbations has also been simulated. This result agrees with experiments and other theoretical results. Our work shows that the lattice Boltzmann model is a useful tool for simulating Rayleigh-Taylor instabilities. An important extension of this work is to develop a lattice Boltzmann model which simulates multicomponent fluids with different densities and very small viscosities.

[1] G. I. Taylor, Proc. R. Soc. London, Ser. A **201**, 192 (1950).

[2] D. H. Sharp, Physica D **12**, 3 (1984).

[3] J. Wang, *Two-dimensional Unsteady Flows and Shock Waves* (Science Press, Beijing, 1995).

[4] D. L. Youngs, Physica D **12**, 32 (1984).

[5] D. L. Youngs, Physica D **37**, 270 (1989).

[6] D. L. Youngs, Phys. Fluids A **3**, 1312 (1991).

[7] J. Glimm and X. L. Li, Phys. Fluids **31**, 2077 (1988).

[8] X. L. Li, Phys. Fluids A **5**, 1904 (1993).

[9] X. L. Li, Phys. Fluids **8**, 336 (1996).

[10] U. Frisch, B. Hasslacher, and Y. Pomeau, Phys. Rev. Lett. **56**, 1505 (1986).

[11] G. R. McNamara and G. Zanetti, Phys. Rev. Lett. **61**, 2332 (1988).

[12] Shiyi Chen and Gary D. Doolen, Annu. Rev. Fluid Mech. **30**, 329 (1998).

[13] A. K. Gunstensen and D. H. Rothman, Physica D **47**, 4320 (1991).

[14] A. K. Gunstensen, D. H. Rothman, S. Zaleski, and G. Zanetti, Phys. Rev. A **43**, 4320 (1991).

[15] X. W. Shan and H. D. Chen, Phys. Rev. E **47**, 1815 (1993).

[16] M. R. Swift, W. R. Osborn, and J. M. Yeomans, Phys. Rev. Lett. **75**, 830 (1995).

[17] D. Grunau, S. Y. Chen, and K. Eggert, Phys. Fluids A **5**, 2557 (1993).

[18] Y. H. Qian, D. d'Humières, and P. Lallemand, Europhys. Lett. **17**, 479 (1992).

[19] Y. H. Qian and Y. F. Deng, Phys. Rev. Lett. **79**, 2742 (1997).

[20] P. Bhatnagar, E. P. Gross, and M. K. Krook, Phys. Rev. **94**, 511 (1954).

[21] Y. H. Qian, Ph.D. dissertation, Ecole Normale Superieure and Université de Paris 6, 1990 (unpublished).

[22] S. Y. Chen, H. D. Chen, D. Martinez, and W. H. Matthaeus, Phys. Rev. Lett. **67**, 3776 (1991).

[23] H. D. Chen, S. Y. Chen, and W. H. Matthaeus, Phys. Rev. A **45**, R5339 (1992).

[24] K. I. Read, Physica D **12**, 45 (1984).

[25] Q. Zhang, Phys. Lett. A **151**, 18 (1990).